Critical behavior of the two-dimensional XY model

Rajan Gupta
T-8, MS-B285, Los Alamos National Laboratory, Los Alamos, New Mexico 87545

Clive F. Baillie
Physics Department, University of Colorado, Boulder, Colorado 80309
(Received 29 August 1991)

We present detailed Monte Carlo results for the susceptibility χ, correlation length ξ, and specific heat C_v for the XY model. The simulations are done on 64^2, 128^2, 256^2, and 512^2 lattices over the temperature range $0.98 \le T \le 1.43$ corresponding to $2 < \xi < 70$. Fits to χ and ξ data favor a Kosterlitz-Thouless (KT) singularity over a second-order transition; however, unconstrained four-parameter KT fits do not confirm the predicted values $\nu=0.5$ and $\eta=0.25$. Our best estimate, $T_c=0.894(5)$, is obtained using KT fits with ν fixed at 0.5. The exponent η is calculated as a function of temperature in the spin-wave phase using Monte Carlo renormalization-group and finite-size-scaling methods. Both methods give consistent results and we find $\eta \approx 0.235$ at $T=0.894$. We also present results for the behavior of vortex density across the transition and exhibit how the dilute-gas approximation breaks down.

I. INTRODUCTION

The classical XY spin model in two dimensions is defined by the Hamiltonian

$$H=\frac{J}{kT}\sum_{\langle ij\rangle}(1-\mathbf{s}_i\cdot\mathbf{s}_j)\equiv\beta\sum_{\langle ij\rangle}(1-\mathbf{s}_i\cdot\mathbf{s}_j)\ , \tag{1}$$

where $\mathbf{s}_i$ is the spin at site i and the sum is over the nearest-neighbor spins. The temperature T is defined in units such that $k=J=1$. This model has an exponential singularity and may describe the critical properties of thin films of superfluid helium.

In a previous study of this model[1] we presented results for the correlation length ξ, susceptibility χ, and the specific heat C_v for the range of temperatures $1.03 < T < 1.43$. The study was carried out on lattices of size 64^2, 128^2, 256^2, and 512^2 using a combination of over-relaxed and Metropolis algorithms. The calculations on the 256^2 and 512^2 lattices were mainly carried out using a parallel computer, the Floating Point Systems T-200 hypercube. For each value of T, the data set were large enough to reduce statistical errors in the measured values of the observables to less than 1%. Careful fits were made to determine the order of the transition using the data for χ and ξ. From these we concluded that the best fit is given by Kosterlitz-Thouless singularity,[2] i.e.,

$$\xi=a_\xi e^{b_\xi t^{-\nu}}\ ,\quad \chi=a_\chi e^{b_\chi t^{-\nu}}\ , \tag{2}$$

where $t=T-T_c$. Our best estimates were $T_c=0.896(1)$ and $\nu=0.500(1)$ where the errors reflect uncorrelated variation of parameters. It should, however, be stressed that data in the range $2<\xi<22$ were barely sufficient to exclude a second-order transition even though the statistical errors were much smaller than 1%.

The leading order KT analysis also predicts the correlation function exponent $\eta=0.25$ where η is defined by

$$\Gamma(r)\sim\frac{1}{r^{d-2+\eta}}\Longrightarrow\chi=c\xi^{2-\eta}\ . \tag{3}$$

Our estimate, however, was $\eta\approx 0.3$ using data in the range $1.03<T<1.1$. Thus we were not able to confirm the KT prediction that $\eta=0.25$ at T_c. If one accepts the hypothesis that η has a strong temperature dependence and the discrepancy is due to the fact that simulations were done far from T_c, then estimates of T_c and ν based on fits given in Eq. (2) are suspect too. The only way to clarify these unresolved issues was to perform simulations closer to T_c.

Recently, Wolff has carried out a similar large lattice simulation extending the temperature range to $0.98<T<1.03$ using a single cluster update algorithm developed by him.[3] The results of the two simulations agree over the range $T\ge 1.03$, but for $T<1.02$, Wolff's results are significantly different from the values obtained by extrapolating our best KT fit results using Eq. (2). While some such deviation is necessary if we are to achieve consistency with all KT predictions, i.e., $\eta=0.25$ at T_c, we find that the actual difference between Wolff's data and extrapolations based on the results of our fits[1] do not go in the direction which improves the estimate of η. (For η to decrease with T the desired behavior is that χ should increase faster relative to ξ since $\chi\sim\xi^{2-\eta}$.)

Wolff's analysis rightly questions the validity of the results we obtained from fits to a limited range, i.e., $T\ge 1.03$. In the present study we show that the χ^2/N_{DF} in these fits is almost constant along a very narrow and flat valley that meanders through the four parameter space (see Figs. 7 and 8). The best estimate of ν is ≈ 0.57 using unconstrained four-parameter KT fit to the χ data and ≈ 0.47 using the ξ data. Because of this difference, we cannot confirm the KT predictions from the fits alone, even though the data cover the range $2<\xi<70$. To confirm or disprove the KT scenario, assuming that the leading KT behavior shown in Eq. (2) has no significant

corrections, requires simulations much closer to T_c. At present our best results are obtained by holding $\nu=0.5$ in the fits, in which case data for both χ and ξ give consistent results with $T_c=0.894(5)$.

This study extends our previous results in a number of ways. (a) We have data down to $T=0.98$ on 512^2 lattices. These new results in the interval $0.98<T<1.02$ are consistent with Wolff's data. (b) We have examined the behavior of vortex density as a function of T over the range $0.7<T<1.25$ and show that the breakdown of the dilute-gas approximation coincides with the location of the specific heat peak at $T\sim 1.04$. (c) We determine η as a function of T using both Monte Carlo renormalization-group (MCRG) and finite-size scaling (FSS) and find that both methods work very well in the spin-wave region. Our final estimate for η is 0.235(5) at $T=0.894$ and the data are consistent with the behavior $\eta(T)=0.25-\alpha(T_c-T)^{1/2}$ close to T_c.

II. PERFORMANCE OF UPDATE ALGORITHMS

A summary of all the data is presented in Tables I–IV. Most of this data are obtained using a combination of over-relaxed and Metropolis algorithms to update the spins. Measurement of observables is made on configurations separated by $N_{\rm or}$ over-relaxed sweeps followed by $N_{\rm met}$ Metropolis sweeps. The over-relaxed algorithm, as described in Ref. 1, consists of reflecting the spin at a given site about Σ, where Σ is the sum of the four nearest-neighbor spins, i.e.,

$$s_{\rm new}=\Sigma s_{\rm old}^{\dagger}\Sigma\ . \tag{4}$$

This implementation of the over-relaxed algorithm[4] is microcanonical and it reduces critical slowing down even though it is a local algorithm. The *hit* elements for the Metropolis algorithm are generated as $e^{i\theta}$, where θ is a uniform random number in the interval $[-\delta,\delta]$ and δ is adjusted to give an acceptance rate of 40–60%. The Metropolis hits make the algorithm ergodic, but their effectiveness is limited to local changes in the energy.

We measure the autocorrelation time for our update procedure by computing $A(n)\equiv\langle M(n)M(0)\rangle$, where M is the total magnetization of the system and n the Monte Carlo time, i.e., the interval between two configurations consisting of $n\times(N_{\rm or}+N_{\rm met})$ sweeps. The decorrelation time τ is defined by the fit $A(n)=\text{const}\times e^{-n/\tau}$ and is given in Tables I–IV (rounded to the nearest integer) along with the statistics. We confirm that, once the lattice size is large enough such that finite-size effects are negligible in observables like χ, τ is independent of L.

The dynamical critical exponent z is defined by $\tau=A\xi^z$. To extract it we plot τ versus ξ on a log-log scale in Fig. 1(a). We find that

$$\tau=0.15\xi^{1.48}\ \text{for}\ N_{\rm or}=8,\ N_{\rm met}=2\ , \tag{5a}$$

$$\tau=0.10\xi^{1.32}\ \text{for}\ N_{\rm or}=16,\ N_{\rm met}=2\ , \tag{5b}$$

$$\tau=0.04\xi^{1.64}\ \text{for}\ N_{\rm or}=14,\ N_{\rm met}=1\ , \tag{5c}$$

for the runs on the FPS T-200 hypercube. The errors on the prefactor and the exponent z are at least 10% due to the statistical errors in determining τ. The systematic errors from making a linear fit to 3–4 data points [as in Fig. 1(a)] are also of similar size. The reason we analyze data

TABLE I. Results for the XY model on $L=64^2$ lattices. Cases for which measurements were not made are left blank. Estimates of ξ in cases where severe finite-size effects are present are not extracted and are indicated with a dash and the corresponding data for χ is marked with an asterisk, and no error estimates are given.

Temp.	Stat.	τ	E	C_v	χ	ξ	$\xi_{\rm av}$	$10^3\rho$	$10^3\bar{\rho}$
1/0.70	200 K	1	0.8296(10)	0.754(7)	12.38(3)	2.25	2.24(2)		
1/0.74	200 K	1	0.8927(10)	0.878(7)	16.78(4)	2.72	2.70(1)		
1/0.78	400 K	1	0.9576(7)	1.002(5)	23.95(4)	3.38	3.37(2)		
1/0.82	290 K	1	1.0243(8)	1.127(7)	36.31(7)	4.33	4.32(2)		
1.10	400 K	2	1.1752(7)	1.393(7)	131.6(3)	9.34	9.31(6)		
1.07	400 K	4	1.2178(7)	1.457(7)	217.5(6)	12.7	12.6(1)		
1.04	300 K	6	1.2623(8)	1.494(8)	392(1)	18.1	18.1(1)		
1.03	490 K	6	1.2772(6)	1.512(7)	476(1)	20.6	20.6(1)		
1.02	200 K	7	1.2922(10)	1.489(9)	574(2)	23.6	23.6(1)	14.0(1)	3.81(5)
1.01	200 K	8	1.3070(10)	1.464(9)	680*	—	—	12.7(1)	3.27(5)
1.00	200 K	8	1.3213(10)	1.409(8)	789*	—	—	11.7(1)	2.93(4)
0.99	200 K	9	1.3353(9)	1.375(7)	894*	—	—	10.6(1)	2.53(4)
0.98	200 K	10	1.3487(9)	1.310(7)	995*	—	—	9.70(9)	2.21(4)
0.97	200 K	10	1.3614(9)	1.260(7)	1082*	—	—		
0.96	200 K	10	1.3738(9)	1.209(6)	1163*	—	—	7.98(8)	1.61(3)
0.95	200 K	10	1.3855(8)	1.159(5)	1234*	—	—	7.29(8)	1.49(3)
0.94	200 K	10	1.3969(8)	1.107(5)	1298*	—	—	6.55(7)	1.19(3)
0.93	200 K	11	1.4081(8)	1.075(5)	1357*	—	—	6.08(7)	1.05(3)
0.92	200 K	11	1.4185(8)	1.034(4)	1408*	—	—	5.53(7)	0.94(2)
0.91	200 K	11	1.4289(7)	1.002(4)	1460*	—	—	5.05(6)	0.78(2)
0.90	200 K	11	1.4388(7)	0.994(4)	1506*	—	—	4.53(6)	0.68(2)
0.89	200 K	12	1.4485(7)	0.968(4)	1550*	—	—	4.14(5)	0.62(2)

TABLE II. Results on $L=128^2$ lattices. Rest is same as in Table I.

Temp.	Stat.	τ	E	C_v	χ	ξ	ξ_{av}	$10^3\,\rho$	$10^3\,\bar{\rho}$
1.25	200 K	1	0.9913(5)	1.068(9)	29.3(1)	3.80	3.80(1)	43.5(1)	13.98(3)
1.16	200 K	1	1.0958(5)	1.267(9)	61.7(2)	5.94	5.94(2)	32.3(1)	10.33(3)
1.13	200 K	1	1.1344(5)	1.322(9)	87.0(2)	7.30	7.30(3)	28.5(1)	9.01(3)
1.10	400 K	2	1.1754(4)	1.383(6)	132.8(3)	9.38	9.40(5)	24.4(1)	7.59(2)
1.07	400 K	4	1.2177(4)	1.445(7)	221.5(6)	12.57	12.55(9)	20.6(1)	6.21(2)
1.04	540 K	8	1.2611(3)	1.453(6)	437(1)	18.7	18.7(1)	16.7(1)	4.81(2)
1.03	980 K	10	1.2758(4)	1.454(6)	572(2)	22.0	22.0(1)		
1.025	100 K	7	1.2831(6)	1.459(11)	666(4)	24.2	24.2(2)		
1.02	100 K	8	1.2902(7)	1.440(14)	768(6)	26.6	26.5(3)	14.2(1)	3.88(2)
1.01	100 K	11	1.3048(7)	1.448(12)	1032(8)	31.3	31.3(3)		
1.00	100 K	13	1.3192(7)	1.421(12)	1422(11)	39.0	38.9(2)		
0.99	100 K	16	1.3333(7)	1.396(12)	1902*	—	—	10.9(1)	2.64(2)
0.98	100 K	18	1.3471(7)	1.367(11)	2418*	—	—		
0.97	400 K	20	1.3602(3)	1.310(5)	2922*	—	—	8.97(3)	2.00(2)
0.96	100 K	21	1.3729(6)	1.233(10)	3409*	—	—		
0.95	100 K	25	1.3850(6)	1.178(9)	3792*	—	—		
0.94	500 K	25	1.3965(3)	1.133(3)	4131*	—	—	6.70(2)	1.27(1)
0.93	200 K	24	1.4076(4)	1.086(5)	4411*	—	—	6.04(3)	1.10(1)
0.92	200 K	24	1.4183(4)	1.056(4)	4663*	—	—	5.54(3)	0.97(1)
0.91	200 K	26	1.4287(4)	1.022(4)	4882*	—	—	5.03(3)	0.83(1)
0.90	200 K	24	1.4387(4)	0.982(4)	5088*	—	—	4.51(3)	0.71(1)
0.89	400 K	28	1.4483(3)	0.964(3)	5279*	—	—	4.09(2)	0.609(7)
0.88	500 K	27	1.4579(2)	0.942(2)	5452*	—	—	3.72(2)	0.524(5)
0.87	300 K	27	1.4671(3)	0.924(3)	5619*	—	—	3.35(2)	0.450(7)
0.86	300 K	27	1.4761(3)	0.894(3)	5771*	—	—	3.06(2)	0.406(6)
0.83	300 K	29	1.5022(2)	0.845(2)	6210*	—	—	2.20(2)	0.245(5)
0.80	300 K	31	1.5268(2)	0.800(2)	6612*	—	—	1.57(1)	0.151(4)
0.75	500 K	70	1.5653(2)	0.743(1)	7244*	—	—	0.84(1)	0.061(2)
0.70	600 K	77	1.6013(2)	0.698(1)	7839*	—	—	0.43(1)	0.022(2)

TABLE III. Results on $L=256^2$ lattices. Rest is same as in Table I.

Temp.	Stat.	τ	E	C_v	χ	ξ	ξ_{av}	$10^3\,\rho$	$10^3\,\bar{\rho}$
1.30	25 K	1	0.9401(7)	0.962(10)	21.9(2)	3.17	3.18(2)		
1.25	75 K	1	0.9908(4)	1.071(8)	29.3(1)	3.80	3.80(1)		
1/0.82	90 K	1	1.0243(4)	1.143(9)	36.4(2)	4.34	4.34(1)		
1.19	112 K	2	1.0585(3)	1.203(9)	46.1(2)	5.01	5.01(2)		
1/0.86	116 K	2	1.0919(3)	1.256(8)	60.0(3)	5.83	5.83(2)		
1.13	122 K	3	1.1344(3)	1.325(9)	87.1(4)	7.30	7.30(2)		
1.10	243 K	4	1.1749(3)	1.404(10)	132.4(5)	9.33	9.32(2)		
1.07	370 K	3	1.2172(2)	1.459(7)	220.8(9)	12.61	12.61(2)		
1.055	575 K	4	1.2389(2)	1.460(5)	302.2(9)	15.23	15.23(5)		
1.04	325 K	5	1.2608(2)	1.459(8)	434(2)	18.8	18.8(3)		
1.03	400 K	6	1.2752(2)	1.458(8)	571(3)	22.2	22.2(2)		
1.025	200 K	8	1.2829(3)	1.443(10)	665(4)	23.9	23.9(2)		
1.02	150 K	9	1.2900(3)	1.442(11)	781(6)	26.4	26.4(2)		
1.01	350 K	13	1.3043(2)	1.429(7)	1092(6)	31.9	31.9(2)	13.15(4)	3.49(2)
1.00	334 K	19	1.3185(2)	1.413(7)	1624(11)	40.5	40.5(3)		
0.99	338 K	29	1.3325(2)	1.375(7)	2491(18)	52.0	51.9(2)		
0.98	280 K	45	1.3462(2)	1.359(6)	3947*	—	—		
0.97	250 K	61	1.3595(2)	1.324(6)	6114*	—	—	9.09(3)	2.05(1)
0.96	320 K	76	1.3725(2)	1.267(5)	8688*	—	—		
0.91	370 K	99	1.4287(1)	1.021(3)	16326*	—	—	5.04(1)	0.834(4)
0.90	570 K	97	1.4388(1)	0.994(2)	17209*	—	—	4.58(1)	0.722(3)
0.89	130 K	99	1.4485(2)	0.972(5)	17983*	—	—	4.18(2)	0.633(6)
0.88	130 K	104	1.4581(2)	0.950(4)	18720*	—	—	3.72(1)	0.526(5)
0.87	130 K	111	1.4673(2)	0.923(4)	19382*	—	—	3.40(1)	0.459(5)

TABLE IV. Results on $L=512^2$ lattices. Rest of the notation is same as in Table I. The update sequences for the four separate runs (A–D) at $T=0.98$ are described in the text. For cases where cluster update was used (sets B–D), the second estimate for χ is obtained using Wolff's improved estimator.

Temp.	Stat.	τ	E	C_v	χ	ξ	ξ_{av}	$10^3\,\rho$	$10^3\,\bar{\rho}$
1.04	210 K	5	1.2605(1)	1.440(9)	433(2)	18.7	18.7(2)		
1.03	230 K	6	1.2750(1)	1.420(9)	564(3)	21.8	21.8(2)		
1.02	175 K	9	1.2900(1)	1.437(9)	779(5)	26.3	26.2(2)	14.33(1)	3.909(6)
1.01	169 K	13	1.3043(1)	1.440(11)	1087(10)	31.8	31.7(3)	13.19(1)	3.488(6)
1.00	271 K	20	1.3185(1)	1.415(7)	1631(12)	40.2	40.3(4)	12.08(1)	3.098(5)
0.99	270 K	31	1.3325(1)	1.369(6)	2520(24)	51.2	51.3(9)	11.04(1)	2.723(4)
0.98	278 K	55	1.3461(1)	1.344(6)	4428(52)	74.3	75(2)	10.05(1)	2.362(6)
A									
0.98	125 K	12	1.3457(1)	1.356(12)	4214(46)	69.1	69(1)		
B					4279(30)				
0.98	75 K	15	1.3457(1)	1.369(16)	4246(60)	69.7	70(1)		
C					4293(42)				
0.98	375 K	19	1.3458(1)	1.407(7)	4260(31)	70.3	70(1)		
D					4256(22)				

separately for each machine architecture is because τ depends on the order in which the lattice is updated. On the FPS T-200 computer it is most efficient to update the lattice by rows, i.e., first all the even spins in a row are updated followed by the odd spins in the same row, with an outer loop over rows.

To obtain a long vector loop on machines like the Cray we sweep across the lattice in a checkerboard pattern, i.e., updating all the even spins on the lattice and then all the odd. For these runs we find that

$$\tau=0.067\xi^{1.62} \quad \text{for } N_{\text{or}}=15,\ N_{\text{met}}=2\ , \tag{6a}$$

$$\tau=0.027\xi^{1.78} \quad \text{for } N_{\text{or}}=20,\ N_{\text{met}}=2\ , \tag{6b}$$

as shown in Fig. 1(b). Thus, the decorrelation time for this algorithm depends on how one sweeps across the lattice in addition to the precise combinations of N_{or} and N_{met} sweeps. A comparison of Eqs. (5b) versus (6a) shows that the lattice decorrelates faster if update is vectorized over rows. This is understandable because in this case information about changed spins propagates from one row to the next within each sweep.

In this paper we correct an error in our previous estimate of the decorrelation time, $\tau=0.10\xi^{1.2}$, presented in Ref. 1. We had inadvertently combined the data from Cray and FPS runs, which have different behavior as shown here.

We have analyzed the dependence of τ on N_{met} and N_{or} in more detail at $T=1.04$ (vortex phase) and $T=0.70$ (spin-wave phase). On a Cray XMP the update time for one Metropolis sweep is 3.78 in units of an over-relaxed sweep, so the computational time per configuration is $t=N_{\text{or}}+3.78N_{\text{met}}$. We plot τt versus N_{or} in Fig. 2 for fixed $N_{\text{met}}=2$ and also versus N_{met} for fixed $N_{\text{or}}=14$. We find that the efficiency of the algorithm increases with N_{or} and the best value is obtained with $N_{\text{met}}=1$. The same conclusion holds for the data at $T=0.70$; deep in the spin wave phase.

Thus, both the prefactor A and the exponent z show a strong dependence on the details of the algorithm. Similar dependence is also seen in the case of the O(3) model.[5] Hence, by careful tuning of N_{met} and N_{or} one can substantially reduce critical slowing down even though the update algorithm is local.

The present update algorithm of choice is Wolff's Cluster algorithm.[3] On a Cray YMP, the ratio of update times per sweep for the over-relaxed, single cluster Wolff, and the Metropolis algorithms are 1:1.66:3.53, respectively. We have data at $T=0.98$ on 512^2 lattice with the following four update sequences: (A) 20 over-relaxed plus 2 Metropolis sweeps, (B) single cluster algorithm of Wolff followed by 5 over-relaxed and 1 Metropolis sweeps, (C) single cluster update followed by 2 over-relaxed and 1 Metropolis sweeps, and (D) single cluster update. Results for these 4 sets are shown separately in Table IV. The autocorrelation time τ for the four cases are 55, 12, 15, and 19 configurations, respectively. From these runs we conclude that the relative efficiency (including CPU time on the Cray YMP) of update using the single cluster algorithm versus 20 over-relaxed plus 1 Metropolis sweeps is ≈ 42 at $\xi=70$.

The second advantage of the cluster algorithm is the possibility of defining improved estimators. For example, one can measure the susceptibility two ways on the same set of lattices: from fluctuations in the total magnetization and using Wolff's improved estimator.[6] These are defined as

$$\chi=\frac{1}{V}\left\langle\left[\sum_i \mathbf{s}_i\right]^2\right\rangle\ ,$$
$$\chi_{\text{imp}}=2\left\langle\frac{1}{C}\left[\sum_{i\in C}\mathbf{r}\cdot\mathbf{s}_i\right]^2\right\rangle\ , \tag{7}$$

respectively. Here C is the cluster of spins flipped about the randomly chosen vector $\mathbf{r}$. We find that both methods give consistent results as shown in Table IV. The errors from the standard method are, however, bigger by a factor of ≈ 1.5. So using the improved estimator gives another factor of 2 in favor of the cluster algorithm.

III. SPECIFIC HEAT

There are two ways to calculate the specific heat: (a) from the fluctuations in the total energy E

$$C_v = \frac{1}{L^2}\beta^2(\langle E^2\rangle - \langle E\rangle^2) \tag{8}$$

and (b) using a numerical derivative of the energy. Here C_v is the specific heat per site. To estimate statistical errors we use a bin size of 500 measurements for method (a) and the full data for method (b). We find that the two methods give consistent results and the data given in Tables I–IV are plotted in Fig. 3. It is clear that (1) the peak occurs at $T \approx 1.04$, well above $T_c \approx 0.9$ and (2) the data for C_v is smooth, i.e., it does not show a divergent behavior or significant finite-size effects. This is consistent with the KT scenario, and makes it unlikely that the system exhibits a normal first- or second-order transition.

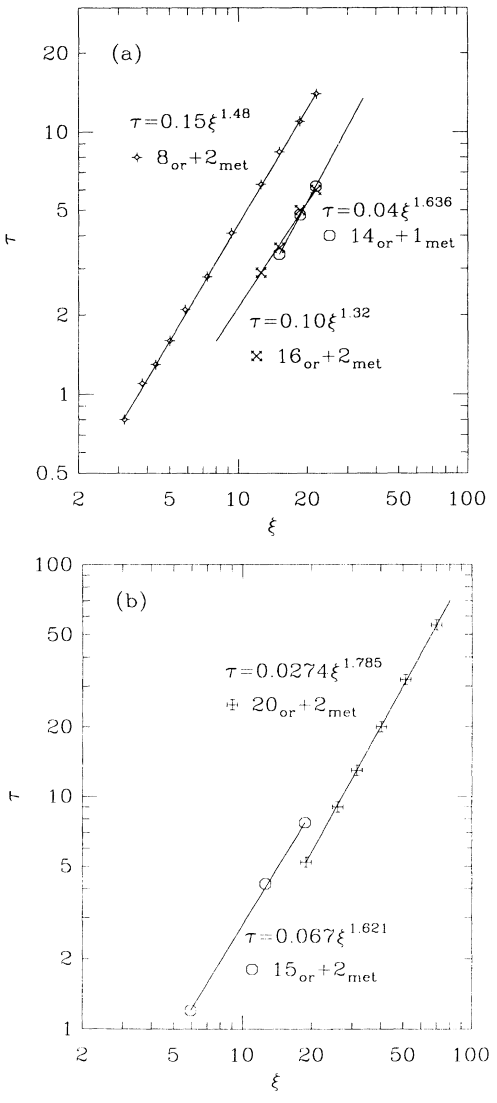

FIG. 1. (a) Plot of the autocorrelation time vs correlation length for data generated on the FPS hypercube. The vectorization was done over even/odd spins in a row. (b) Plot of the autocorrelation time vs correlation length for data generated on a Cray XMP. Vectorization was done over even/odd spins over the whole lattice.

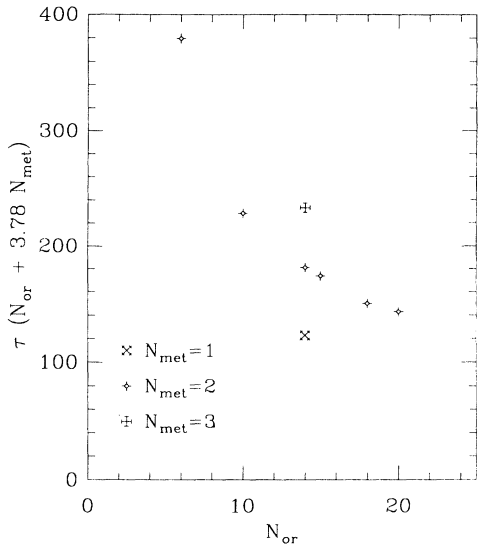

FIG. 2. Comparison of the computer time for producing decorrelated lattices, $\tau \times t$, as a function of N_{met} and N_{or}.

The presence of a peak in C_v does not imply a phase transition. For example, the simple spin-wave model exhibits a maximum in the specific heat even though there are no singularities in the thermodynamic functions. The vortex interactions in the XY model cause the peak to shift to a different value of T. In Sec. VII we examine the behavior of the vortex density as a function of T and

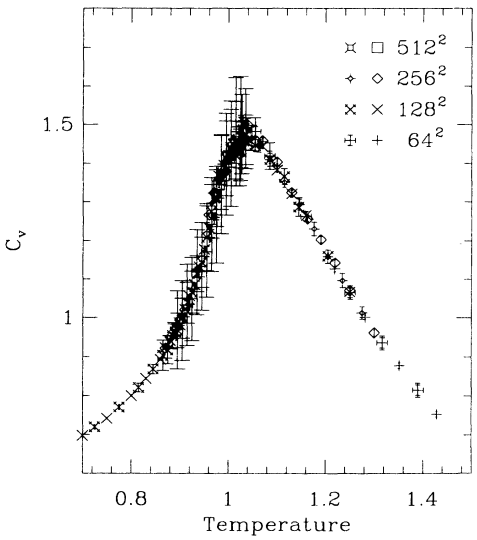

FIG. 3. Plot of the specific heat vs T for data on 64^2, 128^2, 256^2, and 512^2 lattices. We have calculated C_v two different ways as explained in the text and use different symbols to show the data.

show the correlation between the location of this specific heat peak and the breakdown of the dilute gas approximation.

There is significant difference between the four sets of results at $T=0.98$. We believe that critical slowing down, while severely hampering the over-relaxed and Metropolis algorithms, is also present in the cluster update. Thus to get reliable results at and below $T=0.98$ we need a much higher statistics study and further algorithmic improvements. One such possible algorithm is the multigrid Monte Carlo as described in Ref. 7.

IV. CORRELATION LENGTH

We extract the correlation length from the two-point correlation function $\langle O_t O_0 \rangle$ using the following fit:

$$\Gamma(t) \equiv \langle \mathbf{O}_t \cdot \mathbf{O}_0 \rangle = c \cosh[m(L/2-t)] , \tag{9a}$$

where $m \equiv 1/\xi$, and $\mathbf{O}_t$ is the zero-momentum operator

$$\mathbf{O}_t = \sum_x \mathbf{s}(x,t) . \tag{9b}$$

This fit assumes that a single state saturates the two-point correlation function Γ. We verify this by ensuring that the effective mass, defined as

$$m(t) = \ln \frac{\Gamma(t-1)}{\Gamma(t)} , \tag{10}$$

exhibits a plateau corresponding to the asymptotic value. In Eq. (10) we have suppressed the contribution due to periodic boundary conditions for brevity.

In all cases where there is a good signal we observe that a single state dominates the correlation function and that the plateau sets in well before $t=\xi$ and extends to $\approx 3\xi$. We show examples in Fig. 4(a) for the 256^2 lattices and in Fig. 4(b) for the 512^2 lattices. These figures also

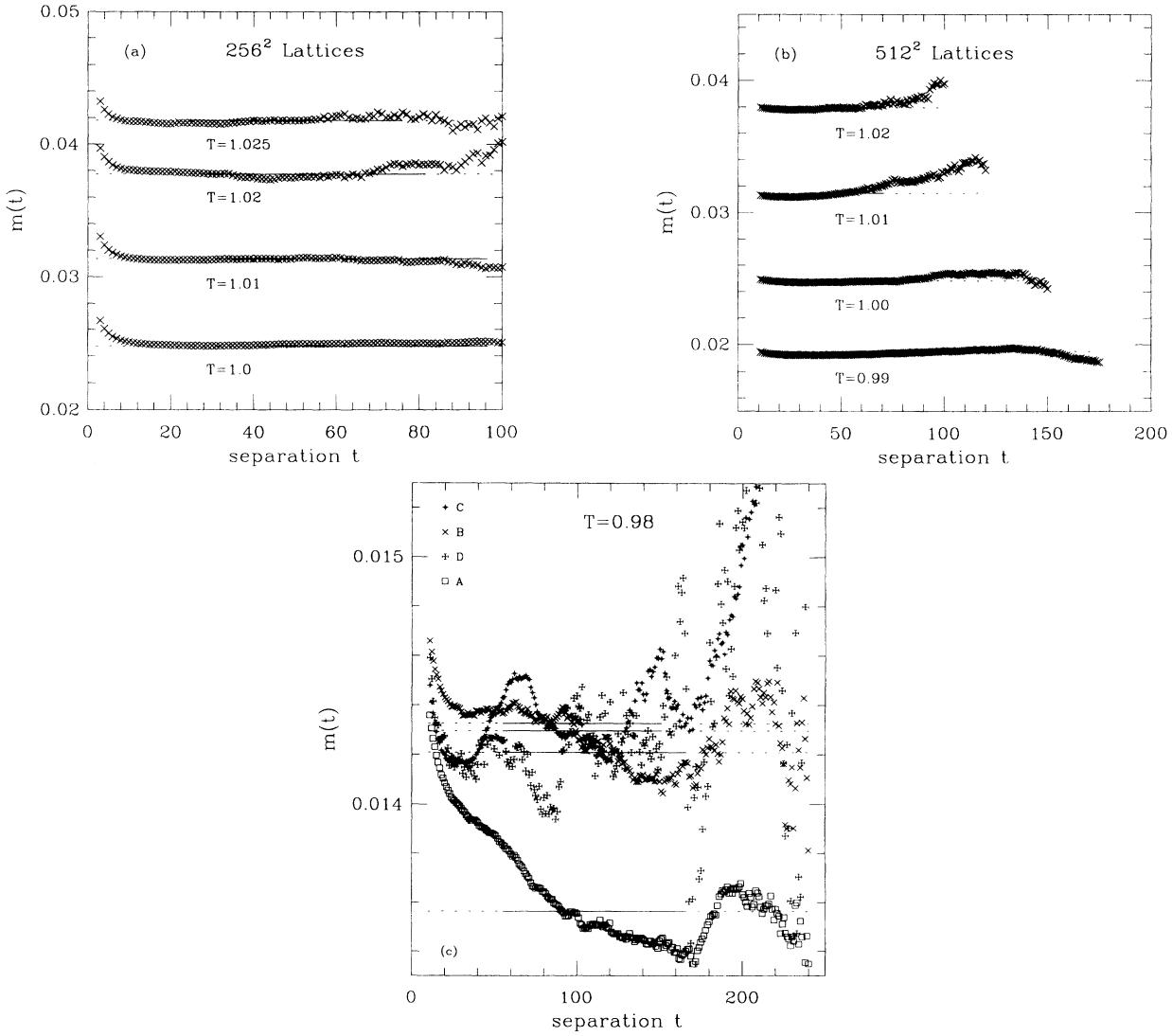

FIG. 4. (a) Plot of effective mass $m(t)$ vs separation t for data on 256^2 lattices. (b) Plot for effective mass $m(t)$ vs separation t for data on 512^2 lattices. (c) Plot of effective mass $m(t)$ vs separation t for data at $T=0.98$ for the four different update sequences, A–D, defined in the text.

show how the plateau degrades due to statistical errors at large t. The solid line in these figures gives the final value of ξ obtained from a one mass fit and is drawn over the range of the fit. Due to an oversight we did not store the covariance matrix so we do not quote an error estimate as the naive χ^2 is not reliable. Overall, we find excellent agreement between our data and that obtained by Wolff.[3]

For comparison, we also list in Tables I–IV an effective correlation length defined by the average

$$\frac{1}{\xi_{\rm av}} = (1/\mathcal{R}) \sum_{t\in\mathcal{R}} m(t) , \tag{11}$$

where $\mathcal{R}$ is the range over which the fit is made. The variance in $m(t)$ over this range is what we quote as the error. The difference between the two values, ξ and $\xi_{\rm av}$ is another measure of errors, including systematic errors due to the contributions from the higher states. Empirically we find that finite-size effects start to become significant when

$$\begin{aligned} &T<1.10 \quad \text{on } 64^2 \text{ lattices} , \\ &T<1.04 \quad \text{on } 128^2 \text{ lattices} , \\ &T<1.01 \quad \text{on } 256^2 \text{ lattices} , \\ &T<0.98 \quad \text{on } 512^2 \text{ lattices} , \end{aligned} \tag{12}$$

as can be seen from the data in Tables I–IV. This suggests a rule of thumb for the XY model: to get infinite volume results the lattice size should satisfy the inequality $L/8>\xi$.

An alternate definition of ξ is given in Ref. 8

$$\xi_k = \frac{L}{2\pi}\left[\frac{\chi}{\chi_k}-1\right]^{1/2} , \tag{13a}$$

where

$$\chi_k = \frac{1}{L^2}\left|\sum_{x,t} \mathbf{s}(x,t) e^{2\pi i x/L}\right|^2 . \tag{13b}$$

This definition of ξ coincides with the pole in the propagator at zero momentum for the free field theory and for a 1D Ising chain. In other nonsolvable models the difference is expected to vanish as ξ becomes large. This definition has the advantage that no fit is needed. (Fits introduce a certain amount of subjectiveness.) We can make direct comparison between the two methods at three values of temperatures where the calculation is done using the same data set

$$\begin{aligned} &\xi=3.80(1); \quad \xi_k=3.82(3) \quad \text{at } T=1.25 , \\ &\xi=18.7(1); \quad \xi_k=18.75(6) \quad \text{at } T=1.04 , \\ &\xi=70.3(6); \quad \xi_k=69.9(8) \quad \text{at } T=0.98 . \end{aligned} \tag{14}$$

The agreement for $T\le 1.25$ suggests that ξ_k is already a good observable for $\xi \ge 4$.

We do find a significant difference in our data at $T=0.98$ between the over-relaxed plus Metropolis update (A) and cluster update (B,C,D) as shown in Table IV. To expose the algorithm dependence further we plot the effective mass for the four update sequences separately in Fig. 4(c). it is clear from this plot that the statistical quality of the over-relaxed plus Metropolis update data is poor, and estimates obtained from this run are unreliable even though the run consists of 7000 units of decorrelation time. We believe that local update algorithms like those utilized in this study stop being practical for $T\le 0.98$. So our best estimate at $T=0.98$ is obtained as a weighted mean of runs B, C, and D.

V. SUSCEPTIBILITY

The magnetic susceptibility is calculated from fluctuations in the magnetization $\mathbf{M}=\sum_{x,t}\mathbf{s}(x,t)$

$$\chi = \frac{1}{L^2}\langle \mathbf{M}\cdot\mathbf{M}\rangle . \tag{15}$$

The data for χ on the four lattice sizes are given in Tables I–IV and the errors are calculated by using a bin size of 500 measurements. We compare data on different lattice sizes to deduce whether our estimates for χ represent infinite volume results. The criteria for obtaining infinite volume results for χ data is consistent with those given in Eq. (12) and our results are in excellent agreement with Wolff's data.[3]

The XY model has a line of fixed points for $T\le T_c$ characterized by the exponent $\eta(T)$. Along this line both χ and ξ diverge with $\chi\propto\xi^{2-\eta}$. On a finite lattice $\xi\sim L$ and finite-size scaling of the χ data can be used to determine η: the slope of the plot $-\ln(\chi/L^2)$ versus $\ln L$ gives $\eta(T)$. Our data near T_c is shown in Fig. 5. We verify that for $T=0.91$, 0.90, and 0.89 the fit is linear using $L=64$, 128, and 256. For $T=0.88$ and 0.87 we extract the slope assuming a linear fit since we have data on 128^2 and 256^2 lattices only. The final data for $\eta(T)$ (including similar data by Wolff[3]) is shown in Fig. 6.

Over the temperature range where χ and ξ data is free of finite corrections, an estimate of η is given by

$$2-\eta = \frac{\ln[\chi(T_1)/\chi(T_2)]}{\ln[\xi(T_1)/\xi(T_2)]} . \tag{16}$$

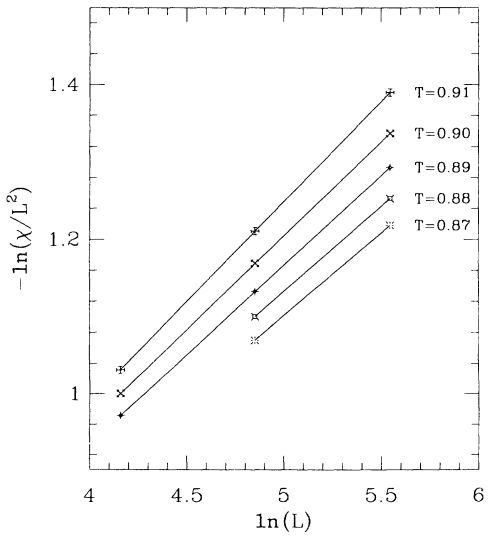

FIG. 5. Finite-size scaling of the susceptibility data.

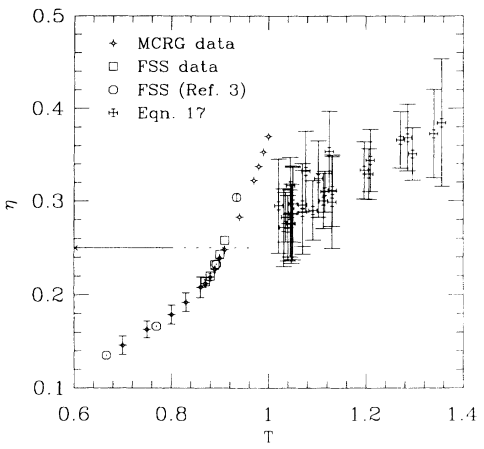

FIG. 6. The correlation function exponent η obtained from MCRG analysis ($\times$), and finite-size scaling ($\diamond$). The data shown with symbol $\circ$ are the finite-size scaling results from Ref. 3. The results using Eq. (16) are shown using the symbol fancy plus.

This definition only requires that $\chi \propto \xi^{2-\eta}$ but is otherwise independent of the kind of singularity. The results shown in Fig. 6 are obtained by performing the following optimization: for every T_1 we choose T_2 such that $|T_1 - T_2|$ as well as the errors in the estimate of η are small.

We postpone a detailed discussion of these results until after we present MCRG results in Sec. VIII. Here we simply note that the behavior of $\eta(T)$ data is compatible with KT prediction assuming $T_c \approx 0.9$.

VI. FITS TO THE DATA USING KT FORM

We present a detailed analysis of the χ and ξ data assuming that the KT form given in Eq. (2) gives the correct critical behavior. In making fits we use the combined data obtained by Wolff[3] and by us. This data set consists of 33 independent points for $T \geq 0.98$ corresponding to $2 < \xi < 70$.

It was discussed in Refs. 1 and 3 that unconstrained four-parameter KT fits to the data are beset by problems of slow convergence due to extremely shallow valleys in the parameter space. Also, it is very hard to estimate errors reliably without allowing all four parameters to vary simultaneously since these are highly correlated. Thus, in order to determine the best fit and to get a profile of the χ^2/N_{DF} we performed the following iterative procedure.

(1) For fixed values of ν and T_c we minimize χ^2/N_{DF} to determine the best value for the constants a and b.

(2) Holding ν fixed, we vary T_c, and repeat step 1. The range of T_c is selected to be large enough to generate a minimum in the χ^2/N_{DF} versus T_c profile.

(3) We repeat step (2) varying ν to get the overall minimum.

The starting values of ν and T_c were varied over the range $0.4 \leq \nu \leq 0.65$ and $0.87 \leq T_c \leq 0.92$. In addition we used a number of random starting points and found that the fit converged to the global minimum given in Table V. We are fairly confident that a different global minimum with a basin of attraction outside this range does not exist.

The results of the best fit are given in the second column of Table V. The quality of the fits is very good; the best fits have a χ^2/N_{DF} of 0.933 and 1.106 for ξ and χ data, respectively, however, the results of the fits for χ and ξ data do not yield the KT answers. Both T_c and ν differ significantly between fits to χ or ξ data and from the KT prediction.

In order to evaluate the significance of this result we show detailed χ^2/N_{DF} profiles in Figs. 7 and 8 for fits to ξ and χ data, respectively. To highlight the narrow valley in the parameters $\chi^2/N_{DF}, \nu, T_c$ we have joined points which were obtained holding ν constant. The figures show that the valley is very flat. What is less evident is that there are a number of local minima along the valley floor at which some minimization programs can get stuck. This map of χ^2/N_{DF} gives us confidence that the

TABLE V. Results of the fits to both χ and ξ data assuming the KT predictions given in Eq. (2). The estimates for the parameters labeled KT are the global minima using all the data. The fits KT1-20, KT9-32, and KT20-70 are based on data with the correlation length in the range $1 \leq \xi \leq 20$, $9 \leq \xi \leq 32$, and $\xi > 20$, respectively. In the latter three fits the value of ν is held fixed at the value obtained in the global fit KT. We give the χ^2/N_{DF} for each fit and an estimate of the exponent η obtained using Eq. (16).

	KT	KT(1–20)	KT(9–32)	KT(20–70)
a_χ	0.4341	0.4303	0.5297	0.4848
b_χ	2.3562	2.3631	2.2473	2.3022
T_c	0.8871	0.8866	0.8918	0.8890
ν	0.5727	0.5727	0.5727	0.5727
χ^2/N_{DF}	1.106	0.833	0.940	2.794
a_ξ	0.1806	0.1779	0.1870	0.1795
b_ξ	1.8727	1.8851	1.8503	1.8777
T_c	0.8953	0.8941	0.8967	0.8950
ν	0.4695	0.4695	0.4695	0.4695
χ^2/N_{DF}	0.933	0.980	1.440	1.373
η	0.74	0.75	0.79	0.77

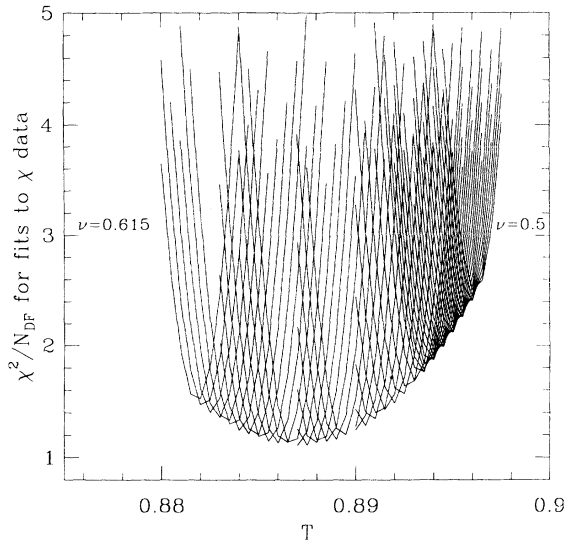

FIG. 7. Profile of χ^2/N_{DF} for KT fits to χ data obtained by holding ν and T_c fixed. The lines join points of constant ν and are drawn to guide the eye.

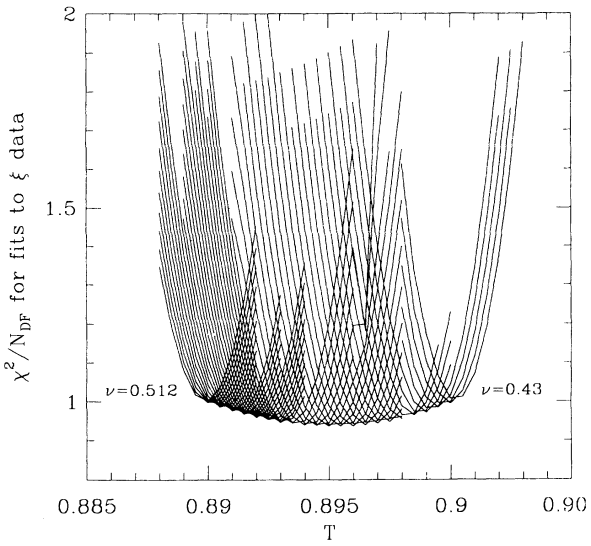

FIG. 8. Profile of χ^2/N_{DF} for KT fits to ξ data obtained by holding ν and T_c fixed. The lines join points of constant ν and are drawn to guide the eye.

numbers quoted in Table V are the true minimum. However, because the valley floor is flat, it is very possible that the location of the global minimum shifts to the parameter values predicted by KT as $T \to T_c$.

We reanalyzed the data fixing $\nu=0.5$ in accord with the KT prediction. The resulting values of the parameters are given in the second column of Table VI. The quality of the fits for ξ is very good as expected from the χ^2/N_{DF} profile. The fit to χ data is not as good, i.e., χ^2/N_{DF} changes from 1.1 to 2.4. In Tables VII and VIII we give the data and the results of the fits with parameter values listed in column 2 of Tables V and VI. The difference between the two fits is comparable to the errors, making it clear why it is not easy to distinguish between them.

To test if fit parameters change as $T \to T_c$ we repeated the above fitting procedure for the three data subsets: $1<\xi<20$, $9\le\xi<32$, and $\xi>20$ which consists of 21, 16, and 12 data points respectively. We now find that fits with four free parameters to these data subsets are not very restrictive. We, therefore, made two separate constrained fits: (1) setting ν to the value given in the second column of Table V and (2) using $\nu=0.5$. The resulting parameter values are given in Tables V and VI for the three cases under labels KT(1–20), KT(9–32), and KT(20–70), respectively.

Another disturbing feature of the unconstrained fits is the value of the exponent η. For KT behavior, using Eqs. (2) and (3), it should be given by

$$\eta=2-\frac{b_\chi}{b_\xi} . \tag{17}$$

The results given in Table V are far from the KT prediction. On the other hand results given in Table VI show much better agreement. Moreover, the deviation from 0.25 decreases as data subsets closer to T_c are analyzed.

We do not give error estimates in Tables V and VI. We caution the reader that in order to reproduce our fits a six-decimal place accuracy is required in the parameters. We have rounded the numbers to four decimal places because the remaining digits are not significant

TABLE VI. Same as Table V except that for all four fits we set $\nu=0.5$ and minimize in the remaining three parameters.

	KT	KT(1–20)	KT(9–32)	KT(20–70)
a_χ	0.2586	0.2739	0.2916	0.2181
b_χ	2.8152	2.7696	2.7425	2.9071
T_c	0.8961	0.8988	0.8990	0.8935
ν	0.5	0.5	0.5	0.5
χ^2/N_{DF}	2.398	1.560	0.912	2.739
a_ξ	0.2129	0.2060	0.2197	0.2197
b_ξ	1.7258	1.7516	1.7062	1.7085
T_c	0.8914	0.8889	0.8927	0.8924
ν	0.5	0.5	0.5	0.5
χ^2/N_{DF}	0.934	0.982	1.441	1.373
η	0.37	0.42	0.39	0.30

even with respect to uncorrelated error estimates. It turns out that if minimization is done with respect to any one of the four parameters (holding the other three at the best fit values) then χ^2/N_{DF} increases by one unit under a change of $\mathcal{O}(5\times10^{-4})$. These uncorrelated estimates were quoted as errors in Ref. 1. This is not correct; realistic estimates have to take into account correlated movement in all four parameters along the valley floor. We do not have a good way of implementing this procedure, so our present best estimate of the errors is the difference between results given in the second column of Table V versus those in Table VI.

For comparison we made similar fits assuming that the critical behavior is described by a second-order transition of the form $\xi=a_\xi(T-T_c)^{-\nu}$. The results of the fit using all the data points are very poor; the $\chi^2/N_{DF}=21.2$ and 224.9 for ξ and χ, respectively. Even if a subset of data points with $\xi>5$ is used we find that $a_\xi=0.668$, $T_c=0.942$, $\nu=1.429$ with $\chi^2/N_{DF}=5.3$, and the corresponding data for χ gives $a_\chi=1.386$, $T_c=0.941$, $\gamma=2.485$ with $\chi^2/N_{DF}=25.9$. Thus we feel confident in ruling out a second-order transition.

To conclude, if we assume that the correct way to analyze the present data ($1\le\xi\le70$) is constrained KT fits, then χ and ξ data give consistent fits with $T_c\approx0.894(5)$ and leave open the possibility that $\eta\to0.25$ as $T\to T_c$. We should briefly mention that it has been argued by Greif, Goodstein, and Silva-Moreira and by Cardy[9] that the leading KT behavior given in Eq. (2) does not set in until $(T-T_c)/T_c\le0.01$. Based on our fit parameters this range of T corresponds to $\xi\ge10^5$, so it will not be possible to test their claim by numerical simulations. However, future calculations that extend the range of data to larger values of ξ will be able to decrease the considerable freedom that we find with four free parameters.

VII. VORTEX DENSITY

In the KT picture the mechanism responsible for the transition is the unbinding of vortices.[2] In the disordered phase ($T>T_c$) the chemical potential for vortex-antivortex pairs is a relevant variable. The density of vortices is large and vortex-antivortex pairs unbind. In the low-temperature phase, vortices are suppressed and

TABLE VII. The final data for χ and the best fit values obtained using the KT parameters given in the second column of Table V (third column) and Table VI (fourth column). Results marked with an asterisk are from Ref. 3.

Temperature	χ data	χ (KT fit: Table V)	χ (KT fit: Table VI)
1.428 571	12.38(03)	12.35	12.25
1.351 351	16.78(04)	16.81	16.78
1.300 000	21.86(16)	21.67	21.71
1.282 051	23.95(04)	23.97	24.03
1.250 000	29.26(12)	29.26	29.38
1.219 512	36.40(18)	36.35	36.54
1.190 000	46.08(18)	46.31	46.57
1.162 791	59.96(27)	59.98	60.31
1.136 364*	80.58(31)	80.39	80.77
1.130 000	87.14(44)	86.90	87.29
1.111 111*	111.43(44)	111.75	112.12
1.100 000	132.41(55)	131.69	132.01
1.098 901*	134.17(45)	133.94	134.25
1.086 956*	162.68(61)	162.58	162.79
1.075 269*	201.29(53)	200.19	200.21
1.070 000	220.84(86)	221.37	221.27
1.063 830*	249.90(80)	250.53	250.26
1.055 000	302.19(89)	302.78	302.16
1.052 632*	319.6(1.1)	319.42	318.68
1.041 670*	414.1(1.7)	416.01	414.62
1.040 000	433.7(2.2)	434.22	432.71
1.030 930*	554.9(2.9)	555.47	553.21
1.030 000	564.1(2.7)	570.46	568.11
1.025 000	665.0(4.0)	661.45	658.64
1.020 410*	764.6(3.0)	763.51	760.29
1.020 000	779(5)	773.65	770.40
1.010 101*	1092(4)	1086	1083
1.010 000	1087(10)	1090	1087
1.000 000*	1604(4)	1610	1609
1.000 000	1631(12)	1610	1609
0.990 000	2520(24)	2521	2532
0.980 390*	4170(19)	4160	4216
0.98	4258(20)	4252	4313

the dominant excitations are spin waves. In two dimensions, these spin waves destroy long-range order,[10] consequently the global O(2) symmetry of the Hamiltonian stays unbroken and there is no net magnetization.

In order to study the behavior of the vortex density we locate the center of all vortices and antivortices using the method described in Ref. 11. A good test of the code is that the number of vortices equals the number of antivortices on each lattice; a consequence of periodic boundary conditions. Measurements were made every 100 configurations. The final data for the vortex density ρ are shown in Tables I–IV. We do not find any significant evidence for finite-size effects, so for each value of T we use all the data and do not distinguish between results obtained on different size lattices.

In the dilute-gas approximation one assumes that vortices are created by thermal fluctuations. There is no interaction between vortices because the separation between pairs is by definition much larger than that between a vortex-antivortex pair. In this limit ρ should behave as

$$\rho \sim \exp\left[\frac{-2\mu}{T}\right], \tag{18}$$

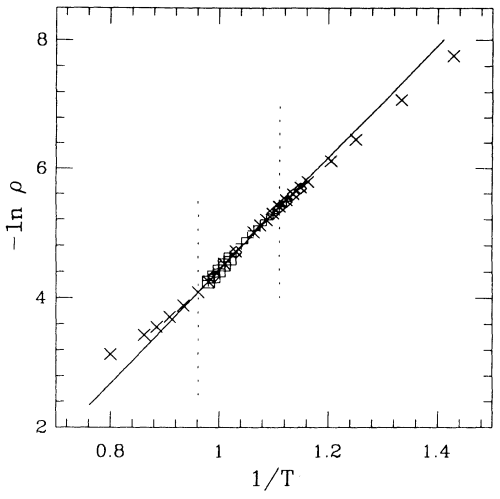

FIG. 9. Plot of the vortex density ρ versus $1/T$. The data are from 64^2 lattices (plus), 128^2 lattices (cross), 256^2 lattices (diamond), 512^2 lattices (square). We divide the data into three regions as explained in the text. The solid line is a linear fit to the intermediate region.

TABLE VIII. The final data for ξ and the best fit values as in Table VII.

Temperature	ξ data	ξ (KT fit: Table V)	ξ (KT fit: Table VI)
1.428 571	2.24(02)	2.24	2.24
1.351 351	2.70(01)	2.71	2.71
1.300 000	3.18(02)	3.17	3.17
1.282 051	3.37(02)	3.37	3.37
1.250 000	3.80(01)	3.80	3.80
1.219 512	4.34(01)	4.33	4.33
1.190 000	5.01(02)	5.01	5.01
1.162 791	5.83(02)	5.85	5.85
1.136 364*	7.01(04)	6.96	6.96
1.130 000	7.30(02)	7.29	7.29
1.111 111*	8.47(06)	8.46	8.46
1.100 000	9.32(02)	9.32	9.32
1.098 901*	9.36(05)	9.41	9.41
1.086 956*	10.69(08)	10.55	10.55
1.075 269*	12.03(06)	11.92	11.92
1.070 000	12.61(02)	12.64	12.64
1.063 830*	13.50(09)	13.58	13.59
1.055 000	15.23(05)	15.17	15.18
1.052 632*	15.61(10)	15.65	15.66
1.041 670*	18.08(13)	18.26	18.27
1.040 000	18.70(20)	18.72	18.73
1.030 930*	21.66(13)	21.60	21.62
1.030 000	21.80(20)	21.93	21.95
1.025 000	23.90(20)	23.90	23.93
1.020 410*	26.37(19)	25.98	26.00
1.020 000	26.20(20)	26.18	26.20
1.010 101*	31.78(21)	31.88	31.90
1.010 000	31.70(30)	31.95	31.97
1.000 000*	40.20(20)	40.07	40.06
1.000 000	40.40(40)	40.07	40.06
0.990 000	51.30(90)	52.00	51.92
0.980 390*	69.27(59)	69.60	69.33
0.98	70(1)	70.50	70.22

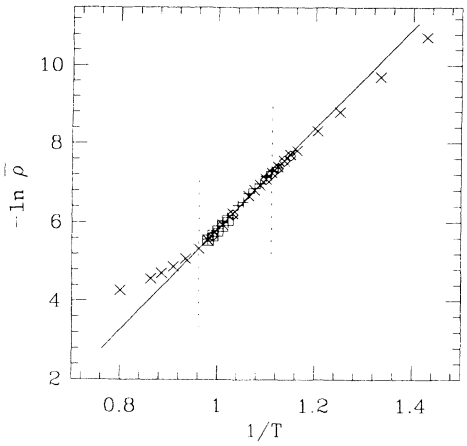

FIG. 10. Plot of the reduced vortex density $\bar{\rho}$ defined in the text versus $1/T$. The three regions and notation are as in Fig. 9. The solid line is a linear fit to the intermediate region.

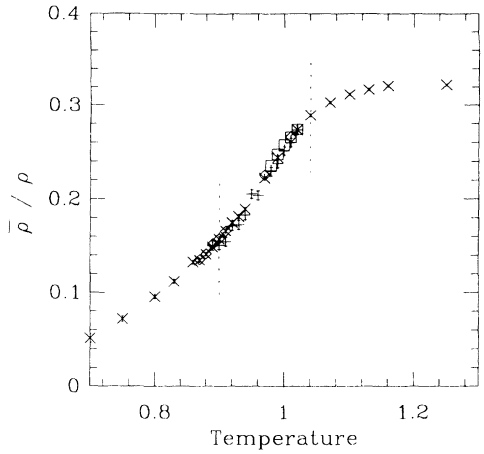

FIG. 11. Plot of the ratio of the reduced vortex density $\bar{\rho}$ to ρ vs T. The three regions and notation are as in Figs. 9 and 10.

where 2μ is the chemical potential for creating a vortex-antivortex pair. To test this hypothesis we plot $\log\rho$ versus $1/T$ in Fig. 9. The data has been divided into three regions: low temperature ($T<T_c$), intermediate temperature ($T_c<T<1.04$), and high temperature ($T>1.04$) region with T_c taken to be 0.9. We estimate $2\mu=7.55$ for $T<T_c$ using a linear fit to the data; to be compared with the KT prediction of 10.2. In the intermediate region, one can still make a good linear fit to the data (shown by the solid line) but with $2\mu=8.82$; slightly larger than the spin-wave value estimated above. A linear behavior in this region suggests that the dilute-gas approximation remains valid, while the increase in 2μ can be attributed to the fact that the pairs are less tightly bound. In the high-temperature region μ decreases rapidly. This signals the onset of disorder, pairs disassociate and it is easy to create another pair. It is interesting to note that the position of the specific heat peak coincides with the onset of the high-temperature region, i.e., $T\sim1.04$.

We also look at a reduced vortex density $\bar{\rho}$. It is defined as one in which all vortex-antivortex pairs that lie on either nearest-neighbor or nearest-neighbor diagonal sites are excluded from the count. The goal is to examine the temperature dependence of pairs that are separated by at least two lattice units. In Fig. 10 we show a plot of $\ln\bar{\rho}$ versus $1/T$. Again, for $T<0.9$ we can make a linear fit with $2\bar{\mu}=10.96$. Compared to $\mu=7.55$, this larger value is consistent with the expectation that the chemical potential for producing separated pairs is larger. In the intermediate region we get $2\bar{\mu}=12.8$, again larger than the value in the spin wave region.

In Fig. 11 we plot $\bar{\rho}/\rho$ versus T. For $T<0.9$ most of the vortices are tightly bound pairs, for $0.9<T<1.04$ we observe a crossover region while for $T>1.04$ the vortices unbind. In our opinion Fig. 11 helps establish that over the interval $0.9<T<1.04$ the vortex density goes smoothly from a dilute gas of tightly bound pairs to a gas of disassociated pairs.

VIII. MCRG ANALYSIS

In our first paper[1] we determined the exponent η only from fits to χ and ξ data. Our best estimate, $\eta\approx0.3$, obtained from using data with $T>1.03$ does not agree with the KT prediction. Since there is a significant variation in the estimate of η with T, it is quite possible for the value of η to converge to the KT prediction as $T\to T_c$. The fact that the predicted value is the same as that for the 2D Ising model, and that $\mathbb{Z}(2)$ perturbations drive the XY model to the Ising fixed point suggests that the MCRG method is a good tool to investigate the critical behavior of the theory for $T\le T_c$.

Earlier calculations show that the MCRG method gives very accurate estimates of η with just a few operators like in the 2D Ising model, i.e., truncation errors are very small.[12] On the other hand MCRG does not give good results for the even exponent ν. We investigate these features in this study by the use of larger lattices, higher statistics and better update algorithm.

We use the standard 2×2 blocking rule, i.e., the block spin is the average of the four spins in a 2×2 block and normalized to lie on the unit circle. On each blocking level we measure the following operators (seven even and five odd):

$E1$	Nearest-neighbor two spin:	$\mathbf{s}(\mathbf{x})\cdot\mathbf{s}(\mathbf{x}+\hat{\mu})$
$E2$	Diagonal two spin:	$\mathbf{s}(\mathbf{x})\cdot\mathbf{s}(\mathbf{x}+\hat{\mu}+\hat{\nu})$
$E3$	Next-nearest-neighbor two spin:	$\mathbf{s}(\mathbf{x})\cdot\mathbf{s}(\mathbf{x}+2\hat{\mu})$
$E4$	Next-nearest-diagonal two spin:	$\mathbf{s}(\mathbf{x})\cdot\mathbf{s}(\mathbf{x}+2\hat{\mu}+\hat{\nu})$
$E5$	Second diagonal two spin:	$\mathbf{s}(\mathbf{x})\cdot\mathbf{s}(\mathbf{x}+2\hat{\mu}+2\hat{\nu})$

$E6$	Ordered square four spin:	$\mathbf{s}(\mathbf{x})\cdot\mathbf{s}(\mathbf{x}+\hat{\mu})\mathbf{s}(\mathbf{x}+\hat{\nu})\cdot\mathbf{s}(\mathbf{x}+\hat{\mu}+\hat{\nu})$
$E7$	Vortex operator four spin:	$[1-\mathbf{s}(\mathbf{x})\cdot\mathbf{s}(\mathbf{x}+\hat{\mu}+\hat{\nu})][1-\mathbf{s}(\mathbf{x}+\hat{\mu})\cdot\mathbf{s}(\mathbf{x}+\hat{\nu})]$
$O1$	Single spin:	$s_x(\mathbf{x})$
$O2$	Three spin:	$\mathbf{s}(\mathbf{x})\cdot\mathbf{s}(\mathbf{x}+\hat{\mu})s_x(\mathbf{x}+\hat{\mu}+\hat{\nu})$
$O3$	Three spin:	$\mathbf{s}(\mathbf{x})\cdot\mathbf{s}(\mathbf{x}+\hat{\mu}+\hat{\nu})s_x(\mathbf{x}+\hat{\mu})$
$O4$	Three spin:	$s_x(\mathbf{x})s_x(\mathbf{x}+\hat{\mu})s_x(\mathbf{x}+2\hat{\mu})$
$O5$	Three spin:	$s_x(\mathbf{x})s_x(\mathbf{x}+\hat{\mu})s_x(\mathbf{x}+\hat{\mu}+\hat{\nu})$

The operators as defined above are summed over the lattice sites and we include all distinct rotations and reflections. From these measurements we construct the linearized transformation matrix. The exponents are determined from the eigenvalues as discussed below.

Odd eigenvalues

The correlation function exponent η is given by

$$\eta=d+2-2\frac{\ln\Lambda_m}{\ln^b}\ , \tag{19}$$

where $b=2$ is the blocking factor and Λ_M is the leading odd (magnetic) eigenvalue. Our results are given in Tables IX–XI for lattices of size 128^2, 256^2, and 512^2, respectively. We now discuss the significant features in the data.

For $T\leq 0.91$, the overall trend is that the eigenvalue increases with the blocking level. We find that the value is consistent between blocking levels (3–4) and (4–5), which we take to be the fixed point value. We quote the difference in value between these two highest blocking levels as a measure of the associated systematic error.

Above T_c, the eigenvalue first increases with blocking level and then decreases. We interpret this as a flow initially toward the KT fixed point and then away from it. The value of η listed in Tables IX–XI is extracted from the level with maximum eigenvalue, which we assume lies closest to the fixed point.

Most of the data is obtained using only one odd operator, namely, the single spin operator $O1$. In order to test whether there exist large truncation effects we made a second run at $T=0.9$ on 256^2 lattices keeping three 3 odd operators ($O1$, $O2$, and $O3$). The comparison in Table X shows that truncation errors exist but are significant only at blocking levels 0–1 and 1–2. Only in the runs at $T=0.70$ and 0.75 did we measure all five odd operators. We find that the overall trend on adding more operators is to decrease the eigenvalue: an example of the magnitude of this effect is shown in Table X. Based on our present data we conclude that the truncation errors are smaller than the difference in the eigenvalues between the two highest blocking levels. So the lack of convergence to the fixed point value is the dominant systematic error in the present data.

To estimate statistical errors we have compared results from the two independent runs made at $T=0.90$ on 256^2 lattices. We find that the difference in Λ_m was ≤ 0.005 at the first two levels and ≤ 0.001 at all higher levels. The same is true of results at $T=0.70$ and 0.75 where errors are estimated by dividing the run into four bins. So our conclusion is that the statistical errors in the data are smaller than the truncation errors and errors due to finite number of blocking levels.

The final estimates of η obtained from the MCRG analysis are plotted in Fig. 6 as a function of temperature. We find that MCRG and finite-size scaling methods give consistent results for $T<0.9$. For higher T we believe that both methods have convergence problems and are therefore not very reliable.

From interpolation of the MCRG data we estimate that $\eta=0.233$ at $T_c=0.894$, while the FSS data gives 0.236. These estimates are in good agreement with the results of Biferale and Petronzio[13] who analyze Monte Carlo data using a phenomenological renormalization-group method.

In order to make a comparison with the KT analysis we first summarize their results. In the spin-wave phase, i.e., as $T\to 0$, η depends linearly on T,[2]

$$\eta(T)=\frac{T}{2\pi}\ . \tag{20}$$

Close to T_c the leading behavior is a square-root singularity;

$$\eta(T)=0.25-\alpha(T_c-T)^{1/2}\ . \tag{21}$$

TABLE IX. The leading odd eigenvalue vs blocking level N and temperature T on 128^2 lattices. The values of η are extracted from levels 2–3 and 3–4, except the one marked with a dagger is from 1–2. The results at $T=0.7$ and 0.75 are obtained using all five odd operators, while for the rest only operator $O1$ was measured.

	Leading odd eigenvalue: 128^2 lattices										
N/T	0.70	0.75	0.80	0.830	0.860	0.870	0.880	0.890	0.940	0.970	1.10
0–1	3.607	3.570	3.581	3.558	3.534	3.526	3.518	3.509	3.466	3.438	3.310
1–2	3.749	3.721	3.707	3.688	3.666	3.658	3.650	3.641	3.593	3.559	3.366
2–3	3.790	3.768	3.747	3.729	3.708	3.700	3.691	3.683	3.626	3.579	3.245
3–4	3.802	3.780	3.760	3.743	3.722	3.714	3.704	3.695	3.626	3.556	2.948
η_{2-3}	0.156	0.172	0.189	0.202	0.219	0.225	0.232	0.238	0.283	0.321	0.498†
η_{3-4}	0.146	0.163	0.179	0.192	0.208	0.214	0.222	0.229	0.283		

TABLE X. The leading odd eigenvalue vs blocking level N and temperature T on 256^2 lattices using the single operator $O1$. The values of η are extracted from levels 3–4 and 4–5 except the case marked with an asterisk 2–3. Two independent runs were made at $T=0.90$ and are labeled a and b. The difference between the fifth and sixth columns is the number of operators used in the analysis: The results in the fifth column are obtained with the three operators $O1$, $O2$, and $O3$, while those in the sixth column are with just $O1$. The difference in results between the sixth and seventh columns is a crude estimate of the statistical errors.

	Leading odd eigenvalue: 256^2							
N/T	0.870	0.880	0.890	0.90[a]	0.90[a]	0.90[b]	0.910	0.970
0–1	3.527	3.518	3.510	3.454	3.501	3.501	3.493	3.438
1–2	3.658	3.650	3.641	3.616	3.632	3.632	3.623	3.558
2–3	3.700	3.691	3.682	3.668	3.672	3.672	3.662	3.578
3–4	3.712	3.703	3.693	3.681	3.683	3.682	3.670	3.552
4–5	3.717	3.708	3.697	3.682	3.686	3.685	3.670	3.491
η_{3-4}	0.216	0.223	0.230	0.240	0.238	0.239	0.248	0.32*
η_{4-5}	0.212	0.219	0.227	0.239	0.236	0.237	0.248	

In addition, vortex interactions give rise to logarithmic corrections; the correlation function at KT point is

$$\Gamma(x)\sim\frac{C(\ln x)^{1/8}}{x^{1/4}}\ , \tag{22}$$

which decays slower than $x^{-1/4}$. Thus η, defined as

$$\eta\sim\frac{-\ln\Gamma(x)}{\ln x}\ \text{as}\ x\to\infty\ , \tag{23}$$

would converge from below if these corrections were not included, as, for example, in our FSS analysis. In the MCRG method logarithmic corrections usually lead to slow convergence.

We plot $[0.25-\eta(T)]^2$ versus T in Fig. 12 in order to test the relation given in Eq. (21). We use both MCRG and FSS data lying in the interval $0.85<T\leq 0.9$. The data are consistent with the singularity predicted in Eq. (12) and from the fit we get a second estimate, $T_c=0.901(10)$.

In order to evaluate whether our results for η confirm the KT scenario we need to consider the following systematic errors.

(1) There is some uncertainty in the determination of T_c. Our best estimate of T_c has been obtained from constrained fits to ξ and χ data.

(2) The desired eigenvalue corresponding to $\eta=0.25$ is $\Lambda_m=3.668$. Our best estimate at $T=0.894$ is $\Lambda_m=3.689$ with just three operators. It is very possible that such a difference is due to lack of convergence, truncation in the number of operators and statistical errors.

TABLE XI. The leading odd eigenvalue vs blocking level N and temperature T on 512^2 lattices. The values of η are extracted from level 2–3 as explained in the text.

	Leading odd eigenvalue: 512^2		
N/T	0.9800	0.9900	1.0000
0–1	3.429	3.419	3.409
1–2	3.545	3.533	3.520
2–3	3.559	3.539	3.519
3–4	3.521	3.489	3.451
4–5	3.434	3.368	3.296
η_{2-3}	0.337	0.353	0.370

In view of these points our overall conclusions are (a) the leading odd eigenvalue is dominated by the single spin operator and (b) MCRG and FSS methods give much better estimates of η than using ξ and χ data [Eqs. (16) and (17)]. The best we can say for the latter analysis is that a linear extrapolation of the results shown in Fig. 6 to $T=0.9$ is compatible with $\eta=0.25$. (c) $\eta\sim 0.25$ at T_c.

Even eigenvalues

The stability of the MCRG method in the even sector is much poorer with respect to truncation errors and convergence with the number of blocking steps. This severe limitation of the calculation is illustrated in Table XII using data obtained on 256^2 lattices at $T=0.9$. We do find that the data show an almost monotonic convergence with the operator order ($E1$, $E7$, $E2$, $E5$, $E4$, $E3$, $E6$), indicating the importance of the vortex operator $E7$. Also, there are no significant finite-size errors even at blocking step $16^2\to 8^2$ as can be ascertained by comparing data on 128^2 and 256^2 lattices.

The final data at different temperature values is given in Table XIII. In cases where data at both 128^2 and 256^2

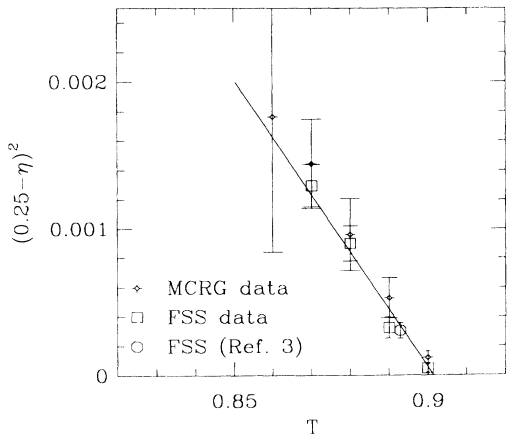

FIG. 12. Plot of $[0.25-\eta(T)]^2$ vs T near T_c. A linear fit has been made to test the KT prediction given in Eq. (21).

TABLE XII. The leading even eigenvalue versus blocking level and the number of operators included in the analysis (we add operators in order shown going from left to right). The results are at $T=0.90$ and on 256^2 lattices. The statistical sample is 100 K and measurements were made every five update sequences.

	Leading even eigenvalue at $T=0.90$ on 256^2 lattices						
Level	E1	E7	E2	E5	E4	E3	E6
0–1	1.66	1.51	1.57	1.49	1.52	1.52	1.51
1–2	1.65	1.58	1.56	1.47	1.48	1.46	1.45
2–3	1.60	1.55	1.48	1.40	1.40	1.37	1.37
3–4	1.54	1.50	1.41	1.26	1.30	1.26	1.27
4–5	1.53	1.49	1.40	1.27	1.28	1.21	1.22

lattices are available we quote results using a weighted mean. By comparing different runs we estimate that the statistical errors in the leading eigenvalue is ≤ 0.05. Thus, the systematic decrease with T and blocking level is statistically significant, however, we find that even the leading eigenvalue becomes complex with three or more operators in most cases. For this reason we feel that the data does not warrant a careful analysis.

According to the KT analysis the leading operator for $T \leq T_c$ is marginal, corresponding to an eigenvalue $\Lambda_t = 1.0$. The best we can say is that the present data is compatible with this prediction. To improve upon these results will require a larger and better set of operators, in addition to high statistics simulations on 1024^2 or larger lattices.

IX. CONCLUSIONS

The single cluster update algorithm is shown to be very efficient compared with local algorithms like the Metropolis and over-relaxed algorithms. Using a combination of these algorithms we have presented infinite volume results for the susceptibility and correlation length for $T \geq 0.98$. The data cover the range $2 < \xi < 70$. In order to push simulations closer to T_c we will require larger lattices (finite-size effects become significant when $L/\xi < 8$) and much better statistics since even the one cluster algorithm does not completely eliminate critical slowing down.

Unconstrained four-parameter fits to susceptibility and correlation length data do not verify the Kosterlitz-Thouless predictions, however, the χ^2/N_{DF} profiles show an almost flat valley in the parameter space. KT fits with ν held fixed at 0.5 give consistent results, from which we estimate T_c to be 0.894(5). The value of η derived from these fits is ≥ 0.3 and suggests that the simulations need to be done much closer to T_c.

We find that fits assuming a second-order transition have $\chi^2/N_{DC} \approx 21$ (ξ data) and 225 (χ data) when all 33 data points are included, i.e., they are significantly worse than KT fits. With the present statistical errors one cannot easily discriminate between the two kinds of fits if a subset of the data is used, say $\xi > 15$. We believe that this lack of resolution will arise any time one has ≤ 20 data points covering a range between ξ and 4ξ and with the errors similar to those in the present calculation.

The best results for η are obtained using the MCRG and finite-size scaling methods. The two methods give consistent results for $T < 0.9$. Combining the results we estimate $\eta = 0.235(5)$ at $T_c = 0.894$. Alternatively, assuming that $\eta = 0.25$ and using the KT scaling form for $\eta(T < T_c)$ we estimate $T_c = 0.901(10)$.

We present a qualitative confirmation of the role played by vortex-antivortex pairs in the KT scenario. We find that the density of pairs shows a crossover in the range $T_c \leq T \leq 1.04$ and during this interval the dilute gas approximation remains valid. The location of the peak in the specific heat, $T \approx 1.04$, coincides with the breakdown of the dilute-gas approximation.

Lastly, using the MCRG method, we find that the vortex operator ($E7$) is important for $T \sim T_c$, however, we are not able to verify that the leading even operator is marginal.

ACKNOWLEDGMENTS

We thank Jerry Delapp for his help with simulations on the FPS machine and Andy White and Ann Hayes for their support of the project. We thank Adrian Patrascioiu for discussions and for bringing Ref. 9 to our notice.

TABLE XIII. The leading even eigenvalue using all seven operators at different blocking levels and at different values of T. Results from 128^2 and 256^2 lattices have been averaged in cases where runs on both lattice sizes were made. The highest blocking level at which measurements were made on 128^2 lattices is 3–4. The statistical sample ranges between 60–100 K and measurements were made every five update sequences.

	Leading even eigenvalue								
Level	$T=0.97$	$T=0.94$	$T=0.91$	$T=0.90$	$T=0.89$	$T=0.88$	$T=0.87$	$T=0.86$	$T=0.83$
0–1	1.47	1.46	1.52	1.51	1.54	1.55	1.57	1.56	1.59
1–2	1.43	1.47	1.42	1.45	1.46	1.48	1.47	1.46	1.46
2–3	1.37	1.36	1.36	1.37	1.36	1.36	1.32	1.29	1.20
3–4	1.32	1.31	1.29	1.27	1.29	1.23	1.21	1.05	1.00
4–5	1.23		1.28	1.22	1.21	1.11	0.96		

The calculations on the Cray XMP were done using a DOE allocation of time at NERSC and at Los Alamos National Lab. The calculations on the Cray YMP were done at PSC and we thank R. Roskies for his generous support. We acknowledge the support of IBM for providing an advanced version of the RS/6000 model 550 work station for this project. The research of CFB is partly supported by DOE Grant Nos. DE-FG03-85ER25009 and DE-AC03-81ER40050, and by AFOSR Grant AFOSR-89-0422.

[1]R. Gupta, J. Delapp, G. G. Batrouni, G. C. Fox, C. F. Baillie, and J. Apostlakis, Phys. Rev. Lett. **61**, 1996 (1988).

[2]J. M. Kosterlitz and D. J. Thouless, J. Phys. C **6**, 1181 (1973); J. M. Kosterlitz, 1046 (1974).

[3]U. Wolff, Nucl. Phys. **B322**, 759 (1989).

[4]M. Creutz, Phys. Rev. D **36**, 515 (1987); F. Brown and T. J. Woch, Phys. Rev. Lett. **58**, 2394 (1987).

[5]J. Apostolakis, C. F. Baillie, and G. C. Fox, Phys. Rev. D **43**, 2687 (1991).

[6]U. Wolff, Nucl. Phys. **B334**, 581 (1990).

[7]R. Edwards, J. Goodman, and A. Sokal, Nucl. Phys. **B354**, 354 (1991).

[8]F. Cooper, B. Freedman, and D. Preston, Nucl. Phys. **B210**, 210 (1982).

[9]J. M. Greif, D. L. Goodstein, and A. F. Silva-Moreira, Phys. Rev. B **25**, 6838 (1982); J. Cardy, *ibid.* **26**, 6311 (1982).

[10]N. D. Mermin and H. Wagner, Phys. Rev. Lett. **17**, 1133 (1966); S. Coleman, Commun. Math. Phys. **31**, 259 (1973).

[11]Jan Tobochnik and G. V. Chester, Phys. Rev. B **20**, 3761 (1979).

[12]P. Harten and P. Suranyi, Nucl. Phys. **B265** [FS15], 615 (1986); R. Swendsen (private communication).

[13]L. Biferale and R. Petronzio, Nucl. Phys. **B328**, 677 (1989).